Supplemental Information

Table of Contents

Table S1. List of antibodies used

Antibody (species-antigen)	*Figure*	*Use*	*Dilution*	*Source*	*Ref.*
Rabbit-KLHL3*	2, 3, 4, 6, S3, S5, S15	WB	1:500	Proteintech,	(1, 2)
	2, S3, S5, S6, S10	IF	1:250	#16951-1-AP	
Rabbit-N-WNK4*	2, 3, 4, 6, S5, S8, S15	WB	1:1000	Ellison Lab	(2-6)
	4, S8, S9, S10	IF	1:4000		
Rabbit-CUL3*	3, 4, 6, S2, S5, S15	WB	1:2000	Bethyl Laboratories,	(3, 7, 8)
				#A301-109A	
Rabbit-NEDD8	3, 6, S5, S15	WB	1:1000	Cell Signaling	(2)
				#2754	
Guinea pig-Parvalbumin	3, 4, 5, S3, S5, S8, S9	IF	1:2000	Swant, #GP72	(2, 3) (6)
Mouse-Calbindin D-28	4, 5, S3, S6, S8, S9	IF	1:2000	Swant, #CB300	(2, 3, 6, 8, 9)
Rabbit-pSPAK^{S373}/pOSR1^{S325*}	4, S8	IF	1:100	Millipore, #07-2273	(10)
Rabbit-pNCC^{T53}*	5, 6, S1, S8, S13, S15	WB	1:2000	Ellison Lab	(2-4, 6, 10-12)
	5	IF	1:1000		
Rabbit-tNCC*	5, 6, S8, S13, S15	WB	1:6000	Ellison Lab	(3, 4, 6, 10-12)
Rabbit-JAB1*	6, S15	WB	1:1000	Santa Cruz	(2-4, 6, 10-12)
				#SC-9074	
Rabbit-β-actin	S1, S3	WB	1:5000	Abcam, #ab8227	(13)
Guinea pig-tNKCC2	S3, S6, S9, S10	IF	1:5000	Bachmann Lab	(3, 4, 11)
Rabbit-RFP	S4, S5	WB	1:1000	Rockland,	(3, 14)
				#600-401-379	

*CUL3, KLHL3, JAB1, NCC, pNCC, KLHL3, pSPAK/pOSR1, and WNK4 antibodies have been validated in knockout mice.

Figure S1

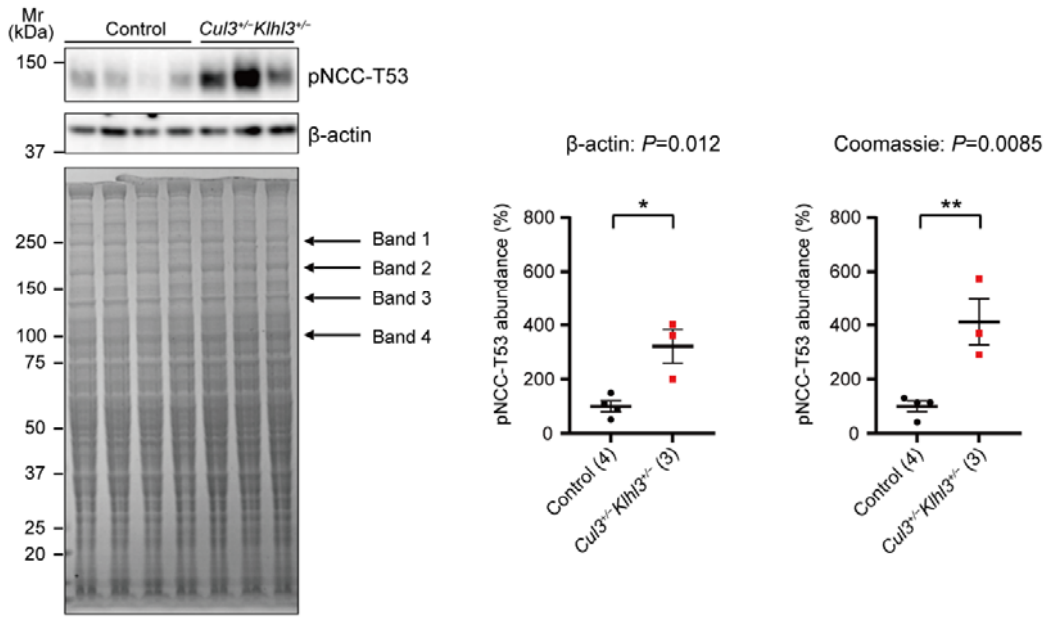

Figure S1. Normalization of Western blot data by Coomassie gel compared with actin normalization. To avoid normalization to actin, which can change abundance in response to experimental manipulation, and reaches saturating levels when as little as 3 µg is loaded per lane, we used the method recommended by McDonough and colleagues (15). An example is shown for phosphorylated Na^+-Cl^- cotransporter (pNCC), but the same approach was used for all blots presented. As previously reported (3, 10), 20 µg (as determined by DC protein assay (Bio-Rad Laboratories, Hercules, CA)) of each sample was resolved on a gel, followed by staining with G-250 Coomassie (Bio-Rad Laboratories). The stained gel was scanned, and four bands were selected (with a molecular weight similar to that of pNCC) for densitometric quantification using ImageJ. Values were normalized to the mean density for that band in all seven samples, defined as 1.0. For pNCC Western blotting, gel loading volumes were then adjusted based on this analysis. The membrane was cut and blotted for pNCC or β-actin. pNCC abundance was normalized to either β-actin or Coomassie (see graphs on right). In this example, variability between the actin and Coomassie approaches was similar, as was the fold-difference in pNCC between control and *Cul3*$^{+/-}$*/Klhl3*$^{+/-}$ mice. Data represent individual values and mean ± SEM relative to controls. Data were examined by two-tailed unpaired t-tests. *, $P < 0.05$; **, $P < 0.01$; (n).

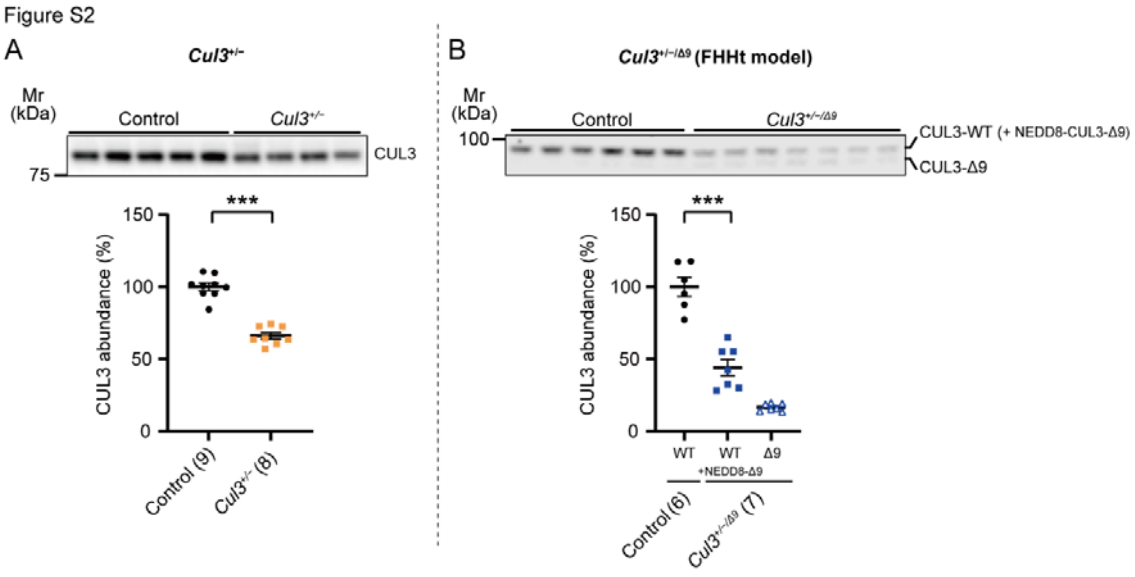

Figure S2. CUL3 expression levels in *Cul3*$^{+/-}$ and *Cul3*$^{+/-/\Delta 9}$ mice. (B and C) Western blotting of whole kidney lysate revealed CUL3 expression levels in (A) *Cul3*$^{+/-}$ and (B) *Cul3*$^{+/-/\Delta 9}$ mice were approximately 40% and 50% lower than each control mice, respectively. In *Cul3*$^{+/-/\Delta 9}$ mice, CUL3-∆9 was detected. Note that CUL3-∆9 with NEDD8-conjugated runs at a similar size to WT CUL3, so in *Cul3*$^{+/-/\Delta 9}$ mice, the upper band represents either WT CUL3 or modified CUL3-∆9. Data represent individual values and mean ± SEM relative to controls. Data were analyzed by two-tailed unpaired t-tests (A and B). ***, $P < 0.001$; (n).

Figure S3

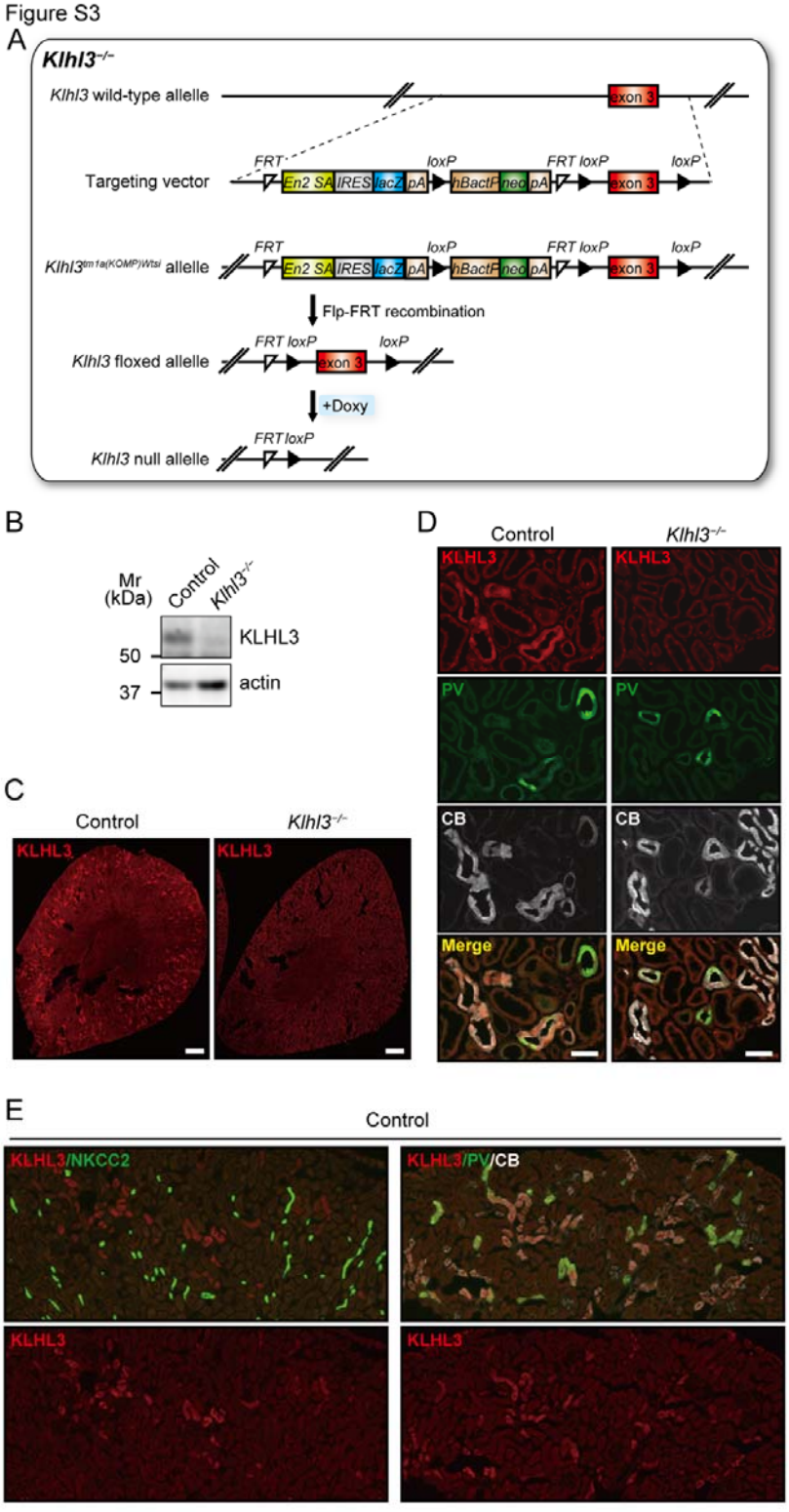

Figure S3. Generation of inducible renal epithelial-specific *Klhl3*$^{-/-}$ mice and anti-KLHL3 antibody validation. (A) Mice carrying a trapping cassette "SA-geo-pA" flanked by the flippase (FLP) recombinase target (FRT) sites upstream from exon 3 of the *Klhl3* allele

(*Klhl3*$^{tm1a(KOMP)Wtsi}$) were generated. After crossing with a mouse expressing Flp recombinase, *Klhl3* floxed allele with exon 3 flanked by Cre recombinase target sites (loxP) were produced. Doxycycline (Doxy, 2 mg/ml in 5% sucrose drinking water vehicle for 3 weeks) treatment induced recombination. Control mice were genetically identical to *Klhl3*$^{-/-}$ mice and were administered vehicle only. (B and C) Anti-KLHL3 antibody specificity was validated by Western blot and immunofluorescence. KLHL3 expression was completely absent in *Klhl3*$^{-/-}$ mice compared with control mice. Scale bars: 500 μm. (D) KLHL3 localization was examined in the distal nephron by co-localization with DCT markers, parvalbumin (DCT1, PV, *green*) and calbindin (DCT2/CNT, CB, *white*). Immunofluorescence revealed strong KLHL3 (*red*) cytoplasmic signal in PV- and CB-positive cells of control mice (*left*). KLHL3 signal was absent in *Klhl3*$^{-/-}$ mice (*right*). (E) Compared with DCT markers (PV and CB), KLHL3 signal was not colocalized with NKCC2, a thick ascending limb marker. Representative image of 1 mouse. Scale bars: 50 μm.

Figure S4

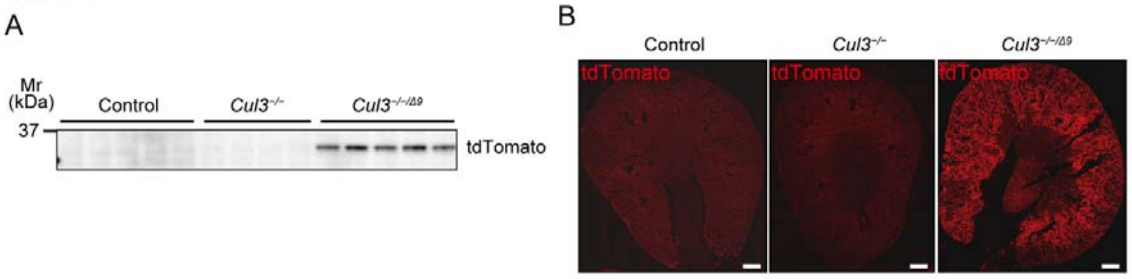

Figure S4. Doxycycline-induced CUL3-Δ9 transgene activation in *Cul3*$^{-/-/\Delta 9}$ mice. (A) Western blotting showed that doxycycline induced tdTomato expression only in *Cul3*$^{-/-/\Delta 9}$ mice. (B) tdTomato fluorescence was observed in renal cortex and medulla only in *Cul3*$^{-/-/\Delta 9}$ mice. Controls were uninduced *Cul3*$^{fl/fl}$ mice, administered 5% sucrose in drinking water. Representative image of 3 mice. Scale bars: 500 μm.

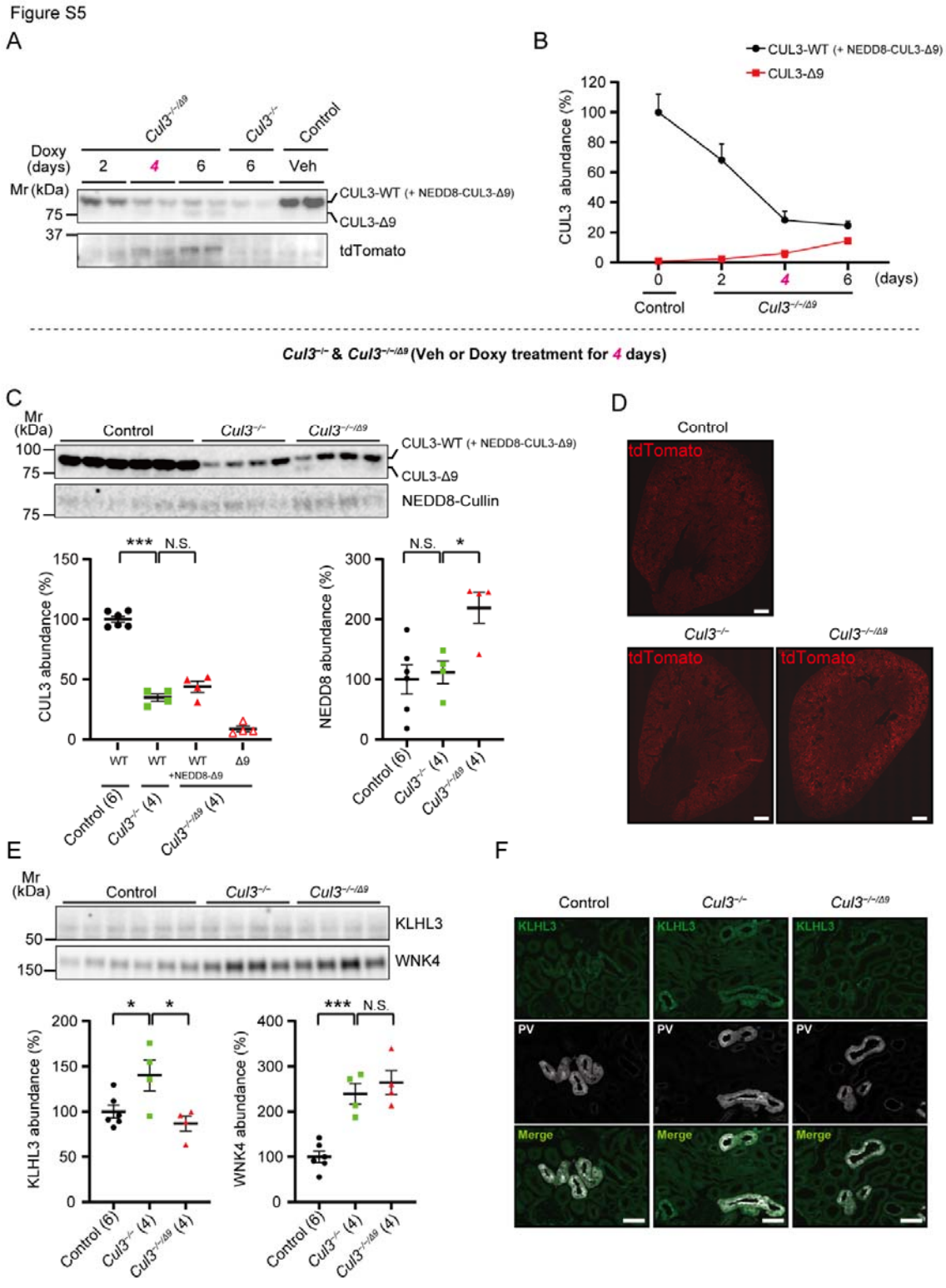

Figure S5. Short-term induction of CUL3-Δ9 is sufficient to degrade KLHL3 and promote WNK4 accumulation. (A and B) Time-course analysis of CUL3 and tdTomato protein expression in response to doxycycline treatment. Mice were treated with doxycycline, kidneys

harvested, then Western blotting performed on lysates. Controls were uninduced *Cul3*$^{fl/fl}$ mice, administered 5% sucrose in drinking water (except for lane 2 in C and E which was *Cul3*$^{fl/fl/\Delta 9}$). Compared with control mice, *Cul3*$^{-/-/\Delta 9}$ mice treated with doxycycline for 4 and 6 days showed lower CUL3 expression and concurrent induction of CUL3-Δ9 and tdTomato with CUL3 disruption. CUL3 expression levels in *Cul3*$^{-/-/\Delta 9}$ mice treated with doxycycline for 6 days were similar to those in *Cul3*$^{-/-}$ mice. (C–F) To determine the effect of CUL3-Δ9 expression on KLHL3 and WNK4 abundances in the acute phase, mice were treated with doxycycline or vehicle for 4 days. (C) Western blotting showed both induced *Cul3*$^{-/-}$ and *Cul3*$^{-/-/\Delta 9}$ mice displayed significantly lower CUL3 abundance than controls, and CUL3 expression did not differ between *Cul3*$^{-/-}$ and *Cul3*$^{-/-/\Delta 9}$ mice. CUL3-Δ9 was detected in only *Cul3*$^{-/-/\Delta 9}$ mice, and NEDD8 was higher in *Cul3*$^{-/-/\Delta 9}$ than in *Cul3*$^{-/-}$ mice. Note that CUL3-Δ9 with NEDD8-conjugated runs at a similar size to WT CUL3, so in *Cul3*$^{-/-/\Delta 9}$ mice, the upper band represents either WT CUL3 or modified CUL3-Δ9. (D) tdTomato fluorescence was observed in only *Cul3*$^{-/-/\Delta 9}$ mice. Scale bars: 500 μm. (E) Western blotting revealed that *Cul3*$^{-/-}$ mice displayed slightly higher KLHL3 protein abundance compared with controls, but *Cul3*$^{-/-/\Delta 9}$ mice did not, indicating KLHL3 abundance is decreased in the early phase of CUL3-Δ9 expression. WNK4 protein abundance was increased in both *Cul3*$^{-/-}$ and *Cul3*$^{-/-/\Delta 9}$ mice. For C) and (E) individual values and means ± SEM are shown. Statistical differences were examined by one-way ANOVA, followed by post hoc unpaired t-tests with Bonferroni correction (A–G). **, $P < 0.01$; ***, $P < 0.001$; N.S., $P > 0.05$; (n). (F) Immunofluorescence revealed cytoplasmic accumulation of KLHL3 (*green*) and aggregation in puncta along DCT1 (PV (*white*) of *Cul3*$^{-/-}$ mice (*middle*), while KLHL3 was mainly detected in small puncta in *Cul3*$^{-/-/\Delta 9}$ mice (*right*). Representative image, 2–3 mice total were analyzed with similar results. Scale bars: 50 μm.

Figure S6

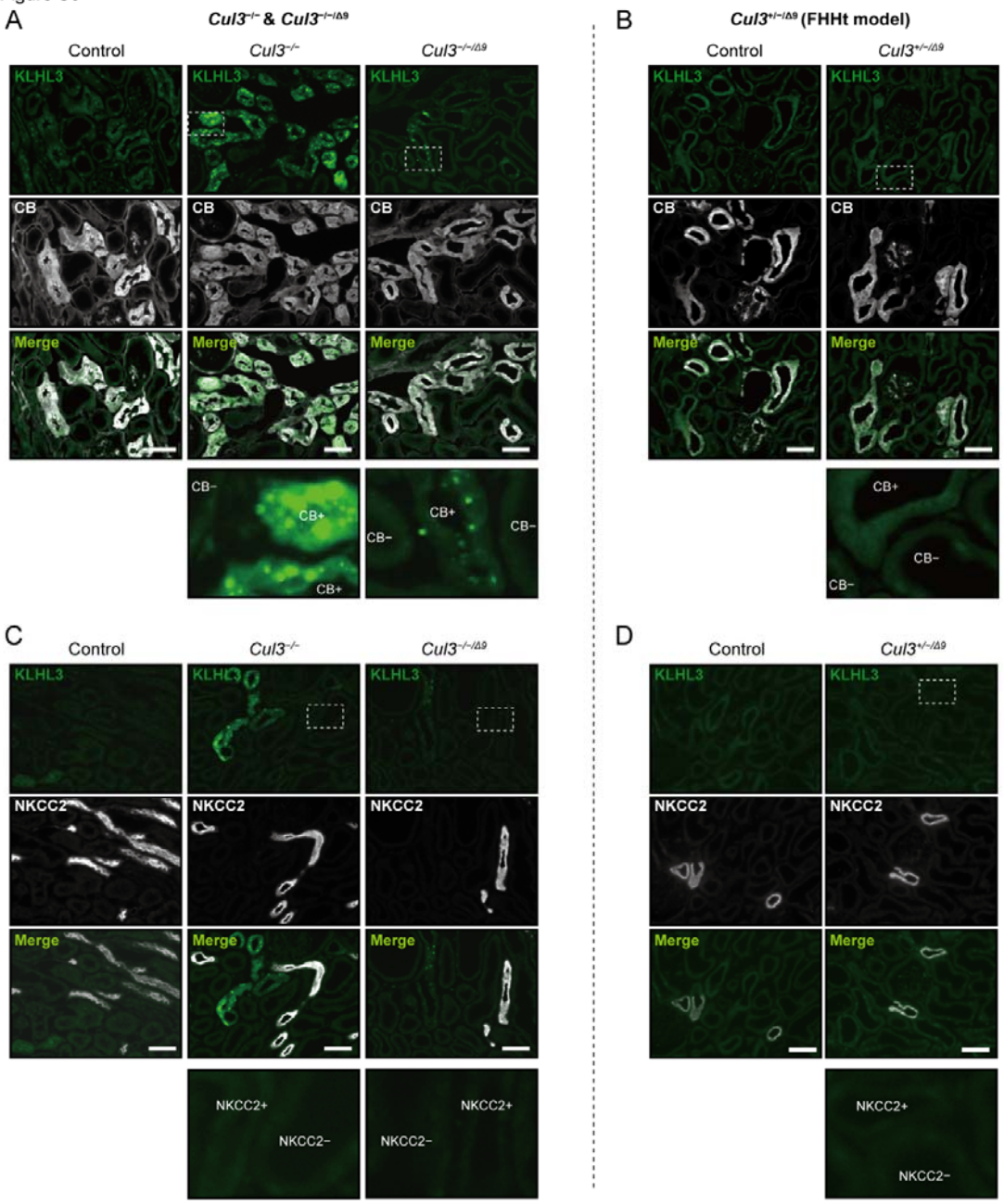

Figure S6. KLHL3 aggregates in DCT of *Cul3*$^{-/-/\Delta 9}$ mice. (A and B) Immunofluorescence revealed cytoplasmic accumulation of KLHL3 (*green*) and aggregation along DCT2 (CB, *white*) of *Cul3*$^{-/-}$ mice, while KLHL3 was mainly detected in aggregates in *Cul3*$^{-/-/\Delta 9}$ mice. In *Cul3*$^{+/-/\Delta 9}$ mice, KLHL3 signal was weaker than in *Cul3*$^{-/-}$ or *Cul3*$^{-/-/\Delta 9}$ mice, but exclusively cytoplasmic, but not aggregated. Controls were uninduced *Cul3*$^{fl/fl}$ mice, administered 5% sucrose in drinking water. (C and D) These changes were not observed along TAL (NKCC2, *white*). Representative image, 3 mice total were analyzed with similar results. Scale bars: 50 μm.

Figure S7

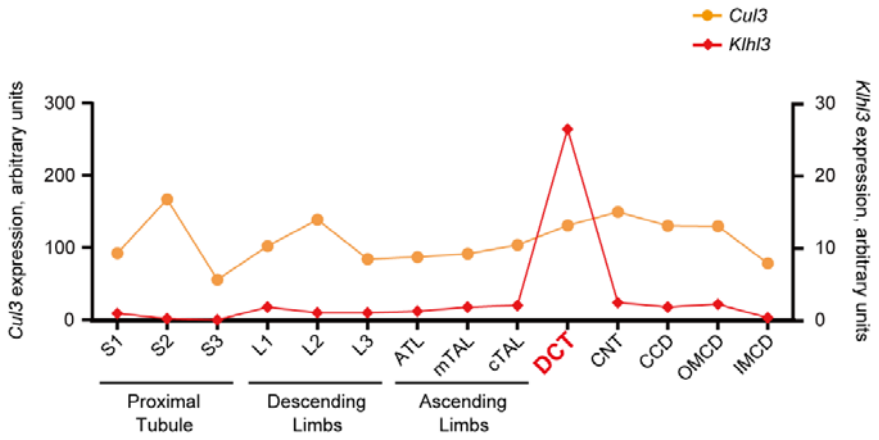

Figure S7. *Cul3* and *Klhl3* expression pattern along the nephron. *Cul3* is expressed along all nephron segments, but *Klhl3* is specifically expressed along DCT. S1–S3, segments of the proximal tubule, L1–L3, segments of the descending limbs, ATL, ascending thin limb; TAL, thick ascending limb; CNT, connecting tubule; CCD, cortical collecting duct; OMCD, outer medullary collecting duct; IMCD, inner medullary collecting duct. Analysis of raw data from https://esbl.nhlbi.nih.gov/MRECA/Nephron/.

Figure S8

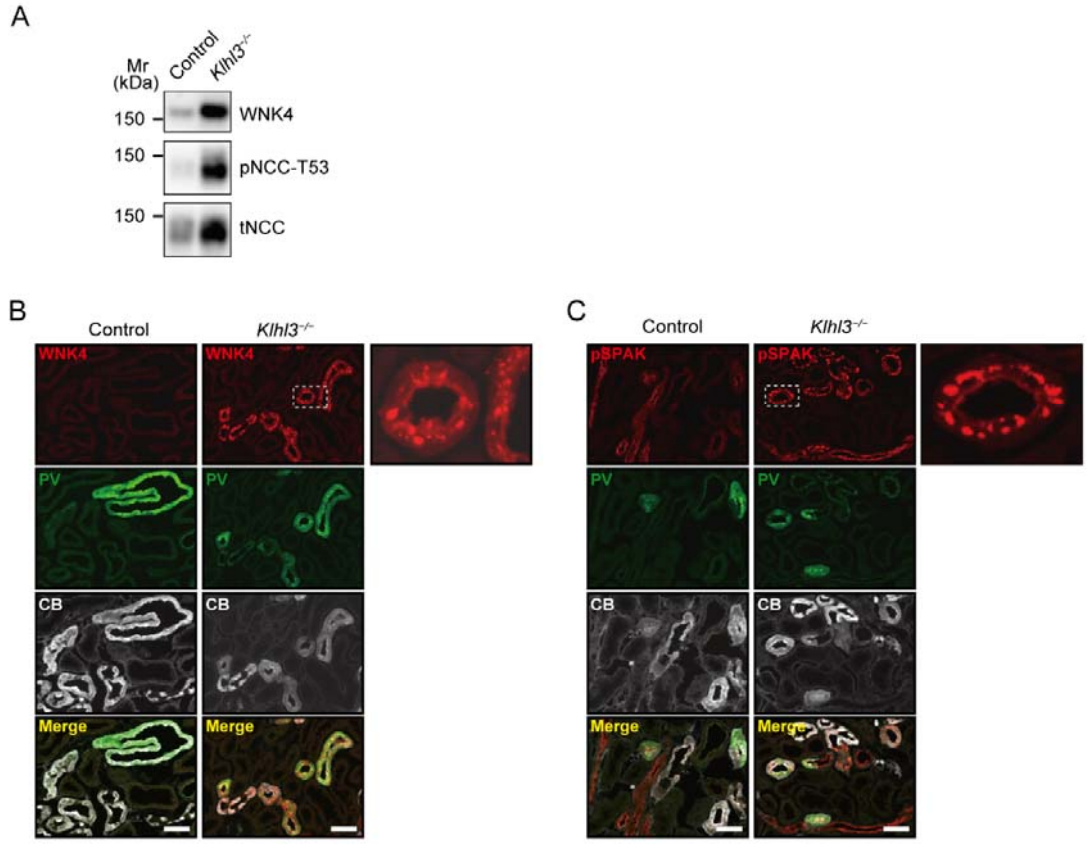

Figure S8. KLHL3 deficiency activates the WNK4-SPAK/NCC cascade. (A) Western blotting showed that WNK4, pNCC-T53, and tNCC protein levels were higher in *Klhl3*$^{-/-}$ mice than in control mice. (B and C) Immunofluorescence showed low WNK4 signal and no WNK4 aggregation in control mice (B, *red*) and no phosphorylated SPAK (pSPAK) aggregation (C, *red*) in the DCT (PV (*green*) and CB (*white*) are markers of DCT1 and DCT2/CNT, respectively). In contrast, WNK4 and pSPAK signal were higher and localized to aggregates in the DCT of *Klhl3*$^{-/-}$ mice. Scale bars: 50 μm.

Figure S9

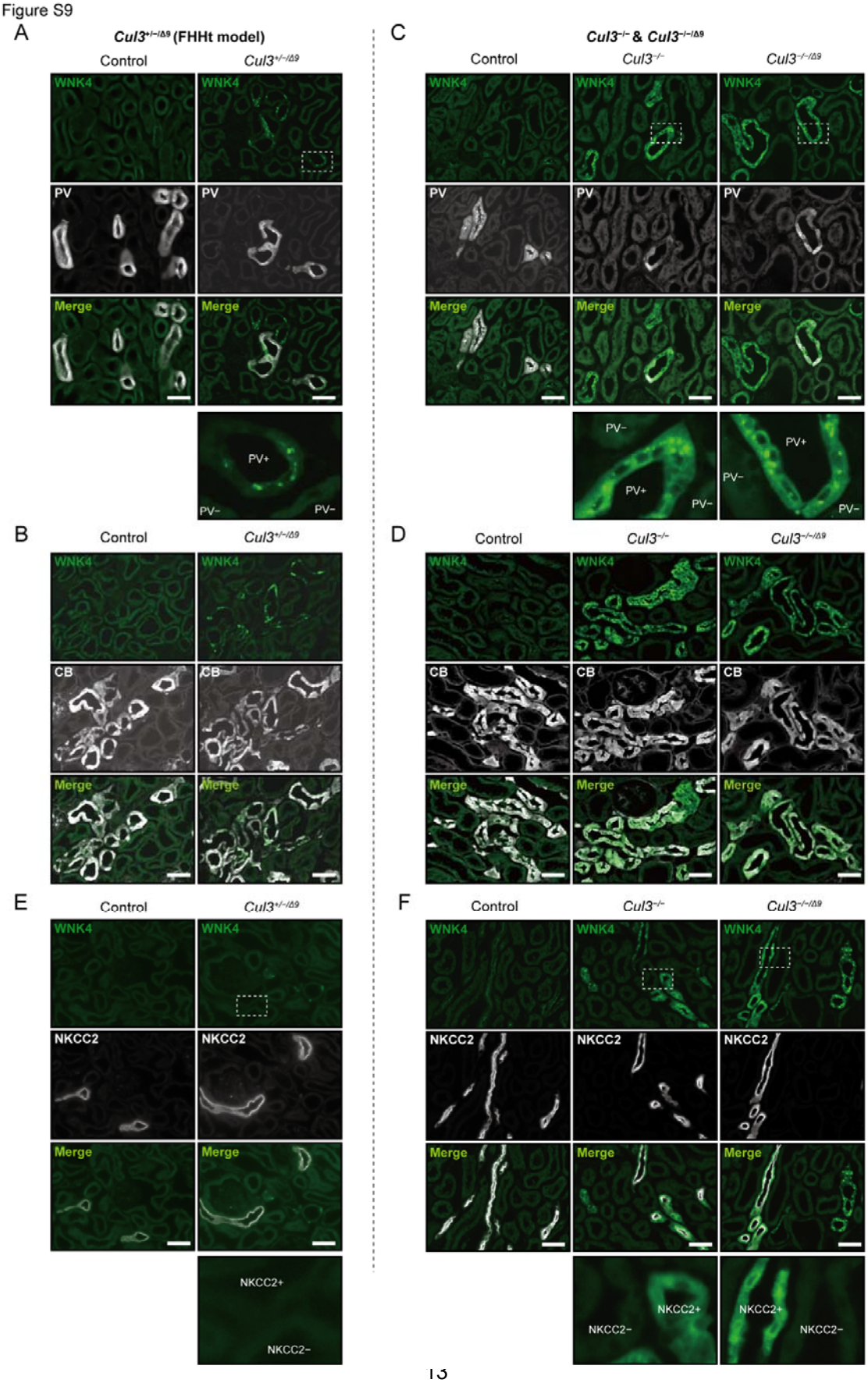
A
Cul3+/−/Δ9 (FHHt model)
Control
Cul3+/−/Δ9
WNK4
PV
Merge
PV+
PV−
C
Cul3−/− & Cul3−/−/Δ9
Control
Cul3−/−
Cul3−/−/Δ9
B
CB
D
E
NKCC2
NKCC2+
NKCC2−
F

Figure S9. WNK aggregation in *Cul3*$^{-/-}$, *Cul3*$^{-/-/\Delta 9}$, and *Cul3*$^{+/-/\Delta 9}$ mice. (A and B) Immunofluorescence showed that *Cul3*$^{+/-/\Delta 9}$ mice showed WNK4 puncta in the DCT1 (PV (A, *white*) and DCT2/CNT (CB (B, *white*). Compared with control mice (*left*), WNK4 signal was high, but appeared weaker than in *Cul3*$^{-/-}$ and *Cul3*$^{-/-/\Delta 9}$ mice (C and D). (C and D) compared with control mice (*left*), WNK4 signal was dramatically higher and localized to puncta in *Cul3*$^{-/-}$ (*middle*), and *Cul3*$^{-/-/\Delta 9}$ (*right*) in the DCT1 (PV (C, *white*) and DCT2 (CB (D, *white*). (E and F) In TAL (*white*), WNK4 accumulated in *Cul3*$^{-/-}$ and *Cul3*$^{-/-/\Delta 9}$ mice (E), but no changes were observed in *Cul3*$^{+/-/\Delta 9}$ mice (F). Controls were uninduced *Cul3*$^{fl/fl}$ mice, administered 5% sucrose in drinking water. Representative image, 3 mice total were analyzed with similar results. Scale bars: 50 μm.

Figure S10

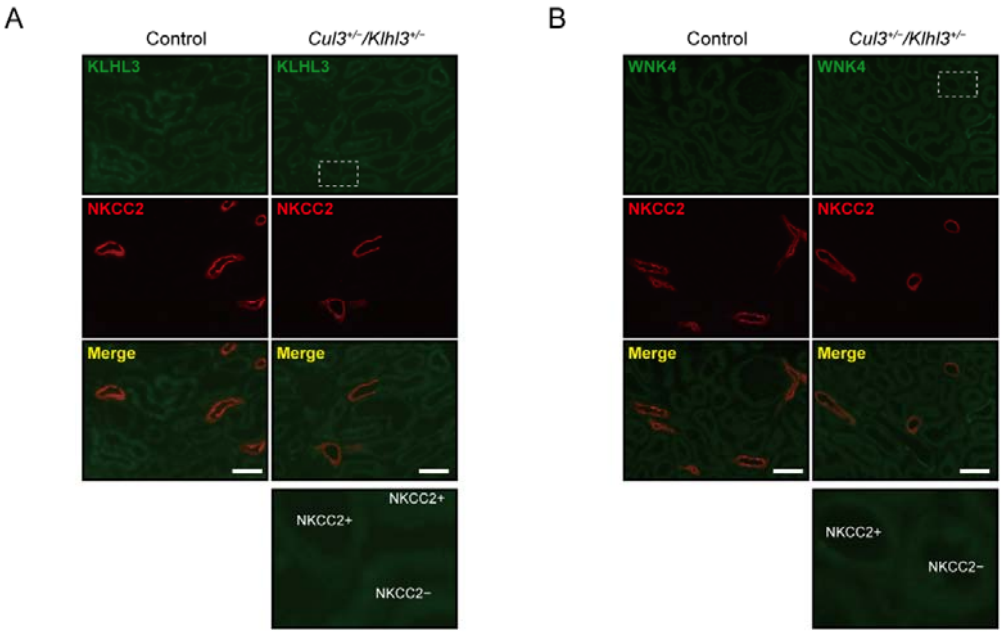

Figure S10. WNK aggregation was not observed along TAL in *Cul3*$^{+/-}$*/Klhl3*$^{+/-}$ mice. (A and B) In TAL (*white*), no changes in KLHL3 (A) and WNK4 (B) signals were observed in *Cul3*$^{+/-}$*/Klhl3*$^{+/-}$ mice, compared with controls. Representative image, 3 mice total were analyzed with similar results. Scale bars: 50 μm.

Figure S11

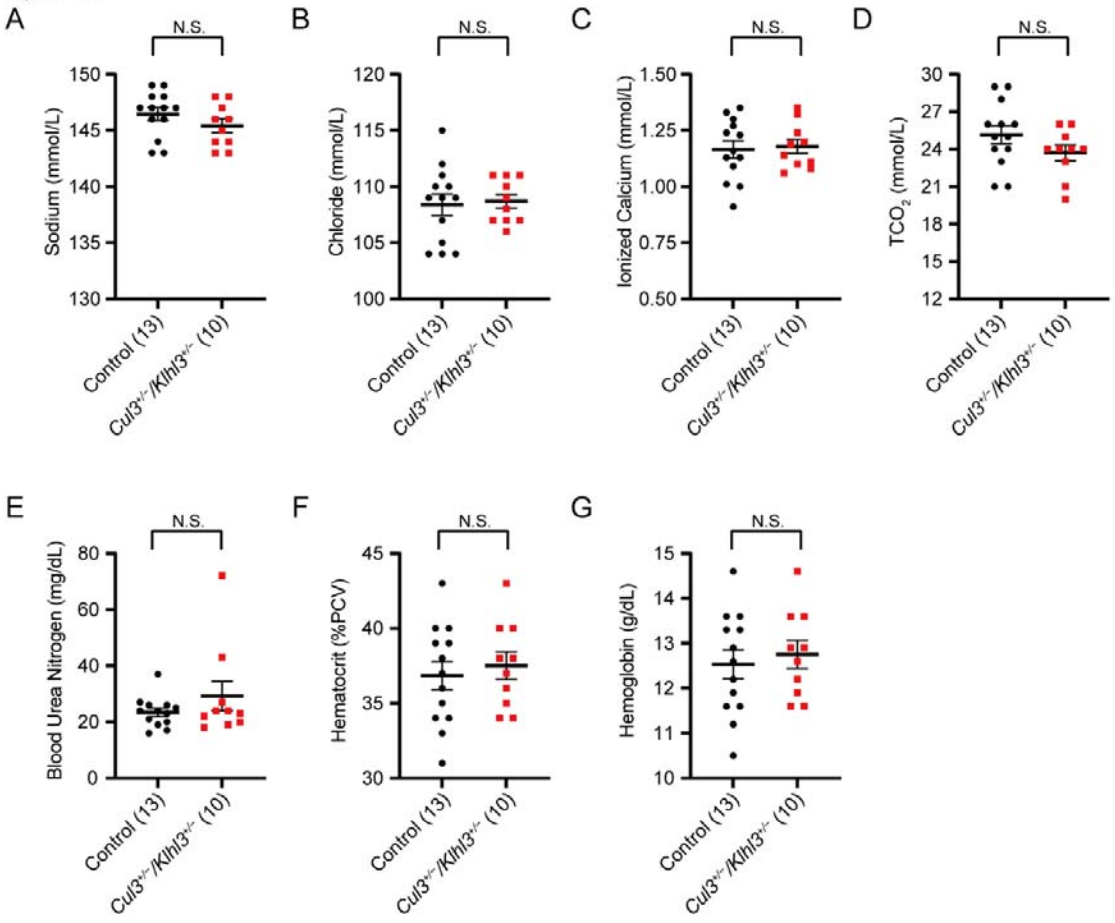

Figure S11. iSTAT analysis of *Cul3*$^{+/-}$/*Klhl3*$^{+/-}$ mice. (A–G) Sodium, chloride, ionized calcium, TCO2, blood urea nitrogen, hematocrit, and hemoglobin did not differ significantly in *Cul3*$^{+/-}$/*Klhl3*$^{+/-}$ mice compared with controls. Data represent individual values and mean ± SEM relative to controls. Data were analyzed by two-tailed unpaired t-tests (A and B). N.S., $P > 0.05$; (n).

Figure S12

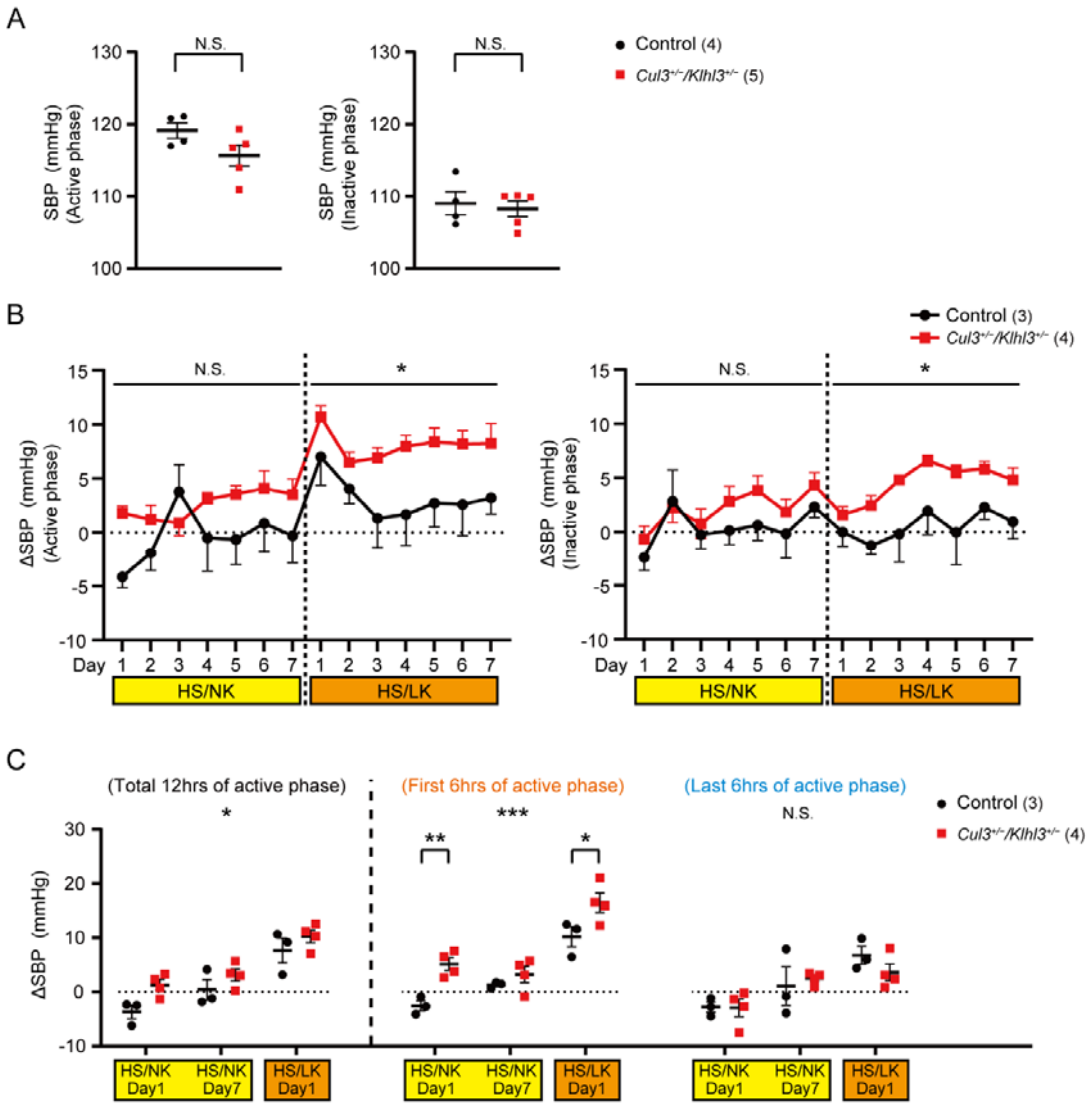

Figure S12. Systolic blood pressure (SBP) is salt-sensitive in male *Cul3*$^{+/-}$*/Klhl3*$^{+/-}$ mice. (A–C) Radiotelemetric blood pressure measurement tracing used for data analyses. After NL diet, mice were fed a high-sodium/normal-K^{+} (HS/NK) diet for 7 days, followed by high-sodium/low-K^{+} (HS/LK) diet for 7 days (**Figure 5D**). (A), using 1 h average values, and the analysis of the mean of the 1 h averages of three dark periods (active phase, *left*) or light periods (inactive phase, *right*) showed that there were no significant differences on normal (NL) diet. (B) and (C) Delta SBP values were calculated as the difference between 12-hr mean SBP of the whole 3 days under NL diet and 12-hr mean SBP under HS/NK or HS/LK diet. (B) When separated into active (*left*) and (*right*) inactive phases, the increase of SBP was significantly higher in *Cul3*$^{+/-}$*/Klhl3*$^{+/-}$ mice the HS/LK diet, but not on the HS/NK diet (although it was significantly higher on HS/NK group when not separated, **Figure 5E**). (C) After changing to HS/NK diet, ΔSBP for the first 6 hrs of active phase (*orange*) was increased in *Cul3*$^{+/-}$*/Klhl3*$^{+/-}$

mice, but decreased in control mice. Changing to HS/LK diet increased ΔSBP for the first 6 hrs of active phase (*orange*) in control mice, but *Cul3*$^{+/-}$*/Klhl3*$^{+/-}$ mice showed higher ΔSBP. For (A) to (C) data present individual values and mean ± SEM relative to controls. N in parentheses. Data were analyzed by two-tailed unpaired t-tests (A), two-way repeated measures ANOVA (B), and two-way ANOVA with Sidak post hoc analysis (C). *, $P < 0.05$; **, $P < 0.01$; ***, $P < 0.001$; N.S., $P > 0.05$.

Figure S13

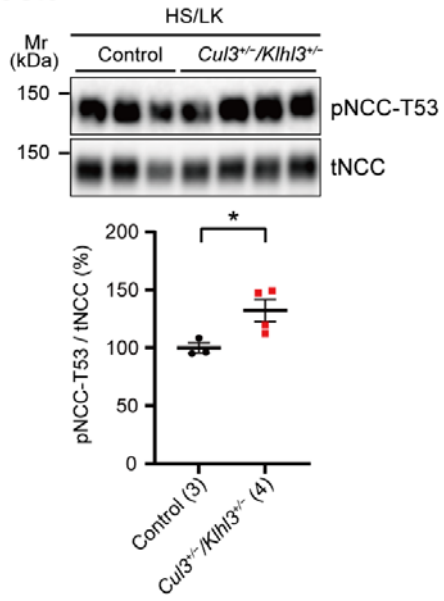

Figure S13. pNCC-T53 and tNCC abundances after high-sodium/low-K^+ (HS/LK) diet for 7 days. Western blotting revealed that the ratio of pNCC-T53 to tNCC was higher in *Cul3*$^{+/-}$*/Klhl3*$^{+/-}$ mice compared with control mice. Data represent individual values and mean ± SEM relative to controls. Data were analyzed by two-tailed unpaired t-test. *, $P < 0.05$; (n).

Figure S14

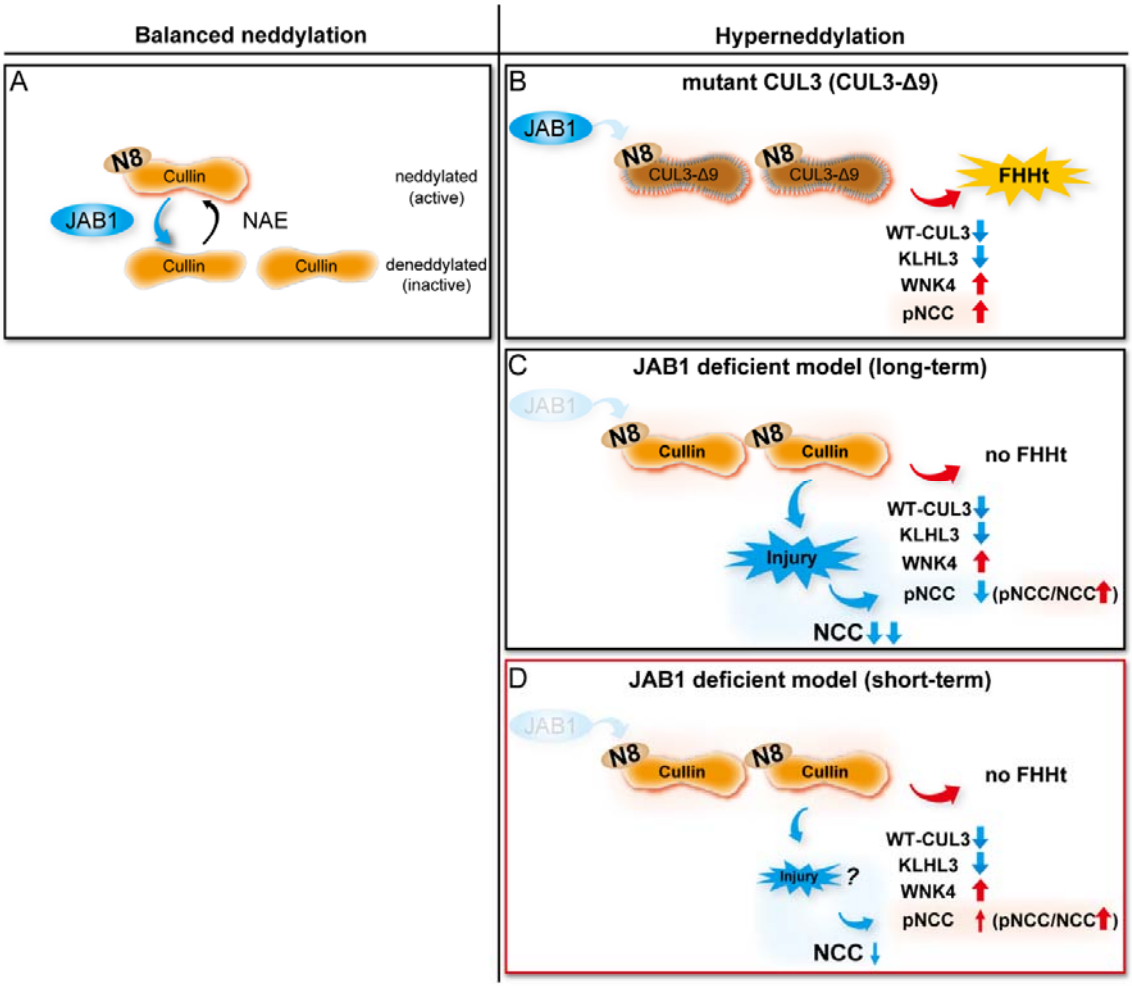

Figure S14. Hyperneddylation of CUL3 causes lowered abundances of CUL3 and KLHL3 and WNK4 accumulation. (A) Cullins are covalently modified by addition of the 9KDa ubiquitin-like protein NEDD8, catalyzed by Nedd9-activating enzyme (NAE). JAB1 catalyzes NEDD8 removal from cullins. Cycling of NEDD8 addition/removal ("neddylation"/"deneddylation") is essential for both the stability and activity of the CUL3-KLHL3 Cullin Ring Ligase. (B–D) "Hyperneddylation" of WT or mutant CUL3 leading to lowered abundances of WT-CUL3 and KLHL3, and WNK4 accumulation are observed in FHHt and JAB1 deficient mouse models. (B) In CUL3-Δ9-mediated FHHt, hyperneddylation results from reduced interaction between CUL3-Δ9 and JAB1. (C) Long-term JAB1 disruption leads to lower NCC and pNCC despite higher pNCC/NCC ratio due to extensive renal injury, so no FHHt phenotype is observed. (D) In short-term JAB1 disruption, NCC expression levels are relatively preserved and pNCC is higher, but again no FHHt phenotype occurs due to effects on other segments.

Figure S15

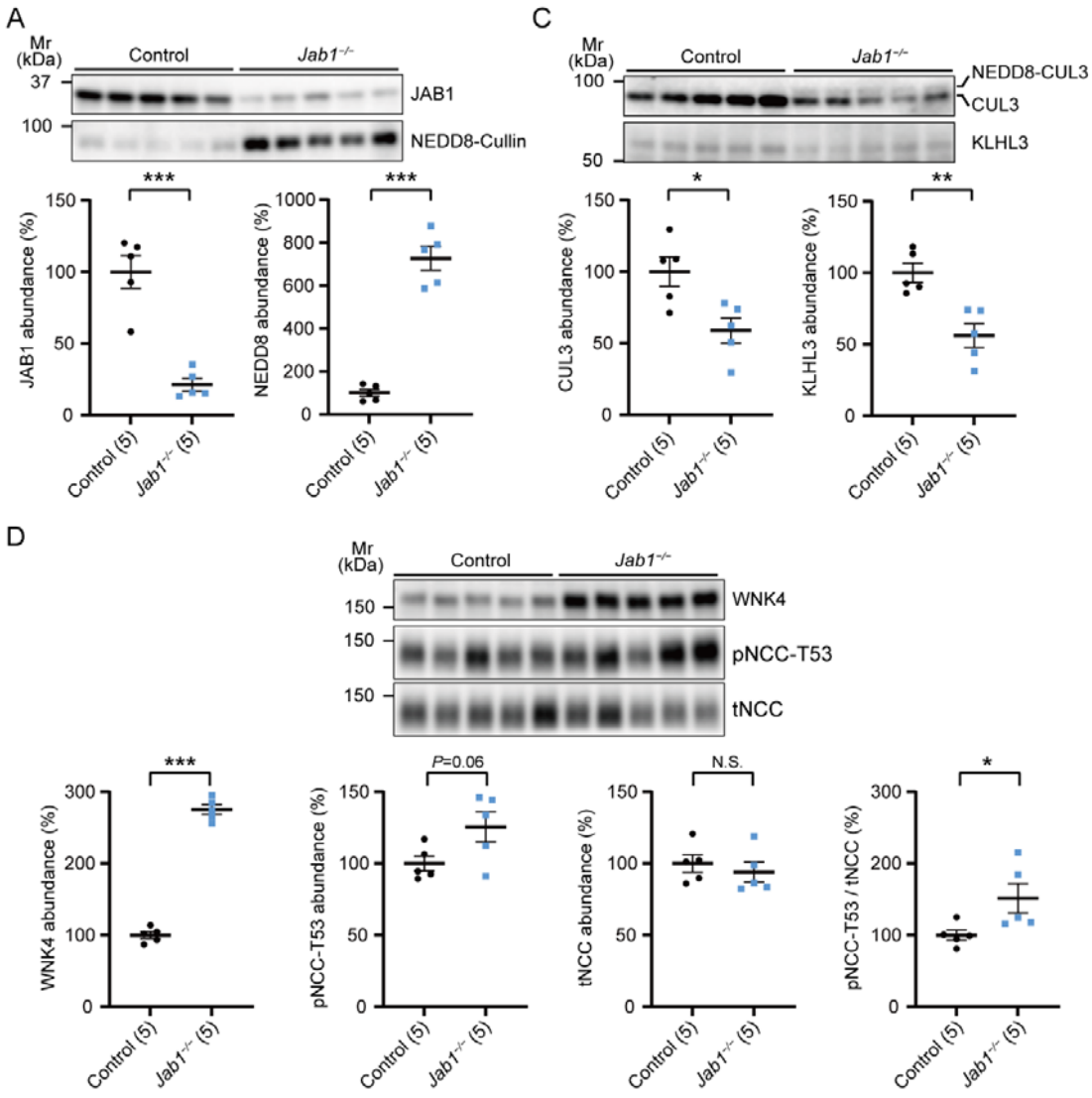

Figure S15. Acute disruption of the deneddylase *Jab1* mimics the effects of CUL3-Δ9 expression. (A) Tubule-specific *Jab1*$^{-/-}$ mice were made by generating mice with two "floxed" *Jab1* alleles and the Pax8-rtTA-LC1 system (18). Mice were treated with doxycycline for 3 weeks to induce recombination to acutely disrupt *Jab1*, then samples collected 1 week after the end of treatment. (B) Western blotting showed that JAB1 expression was significantly reduced, while abundance of neddylated Cullins (NEDD8-Cullin) was increased. (C) *Jab1*$^{-/-}$ mice displayed higher abundance of neddylated CUL3, and abundances of total (neddylated and unneddylated) CUL3 and KLHL3 were about 50% lower than in controls. (E) Abundances of WNK4 was significantly higher, abundance of NCC phosphorylated at T-53 (pNCC-T53) trended higher, but compared with **Figure 6**, total NCC was not different; pNCC-T53/tNCC was significantly higher. Individual values and means ± SEM are shown. Statistical differences were examined by two-tailed unpaired t-tests (B and C). *, $P < 0.05$; **, $P < 0.01$, ***, $P < 0.001$.

Supplemental References

1. Sasaki E, Susa K, Mori T, Isobe K, Araki Y, Inoue Y, et al.: KLHL3 Knockout Mice Reveal the Physiological Role of KLHL3 and the Pathophysiology of Pseudohypoaldosteronism Type II Caused by Mutant KLHL3. *Mol Cell Biol,* 37, 2017 10.1128/MCB.00508-16
2. Cornelius RJ, Si J, Cuevas CA, Nelson JW, Gratreak BDK, Pardi R, et al.: Renal COP9 Signalosome Deficiency Alters CUL3-KLHL3-WNK Signaling Pathway. *J Am Soc Nephrol,* 29**:** 2627-2640, 2018 10.1681/ASN.2018030333
3. Ferdaus MZ, Miller LN, Agbor LN, Saritas T, Singer JD, Sigmund CD, et al.: Mutant Cullin 3 causes familial hyperkalemic hypertension via dominant effects. *JCI Insight,* 2, 2017 10.1172/jci.insight.96700
4. McCormick JA, Yang CL, Zhang C, Davidge B, Blankenstein KI, Terker AS, et al.: Hyperkalemic hypertension-associated cullin 3 promotes WNK signaling by degrading KLHL3. *J Clin Invest,* 124**:** 4723-4736, 2014 10.1172/JCI76126
5. Terker AS, Zhang C, McCormick JA, Lazelle RA, Zhang C, Meermeier NP, et al.: Potassium modulates electrolyte balance and blood pressure through effects on distal cell voltage and chloride. *Cell Metab,* 21**:** 39-50, 2015 10.1016/j.cmet.2014.12.006
6. Terker AS, Castaneda-Bueno M, Ferdaus MZ, Cornelius RJ, Erspamer KJ, Su XT, et al.: With no lysine kinase 4 modulates sodium potassium 2 chloride cotransporter activity in vivo. *Am J Physiol Renal Physiol,* 315**:** F781-F790, 2018 10.1152/ajprenal.00485.2017
7. Agbor LN, Ibeawuchi SC, Hu C, Wu J, Davis DR, Keen HL, et al.: Cullin-3 mutation causes arterial stiffness and hypertension through a vascular smooth muscle mechanism. *JCI Insight,* 1**:** e91015, 2016 10.1172/jci.insight.91015
8. Saritas T, Cuevas CA, Ferdaus MZ, Kuppe C, Kramann R, Moeller MJ, et al.: Disruption of CUL3-mediated ubiquitination causes proximal tubule injury and kidney fibrosis. *Sci Rep,* 9**:** 4596, 2019 10.1038/s41598-019-40795-0
9. Singer JD, Gurian-West M, Clurman B, Roberts JM: Cullin-3 targets cyclin E for ubiquitination and controls S phase in mammalian cells. *Genes Dev,* 13**:** 2375-2387, 1999 10.1101/gad.13.18.2375
10. Ferdaus MZ, Mukherjee A, Nelson JW, Blatt PJ, Miller LN, Terker AS, et al.: Mg(2+) restriction downregulates NCC through NEDD4-2 and prevents its activation by hypokalemia. *Am J Physiol Renal Physiol,* 317**:** F825-F838, 2019 10.1152/ajprenal.00216.2019
11. McCormick JA, Mutig K, Nelson JH, Saritas T, Hoorn EJ, Yang CL, et al.: A SPAK isoform switch modulates renal salt transport and blood pressure. *Cell Metab,* 14**:** 352-364, 2011 10.1016/j.cmet.2011.07.009
12. Ferdaus MZ, Barber KW, Lopez-Cayuqueo KI, Terker AS, Argaiz ER, Gassaway BM, et al.:

SPAK and OSR1 play essential roles in potassium homeostasis through actions on the distal convoluted tubule. *J Physiol,* 594**:** 4945-4966, 2016 10.1113/JP272311

13. Cornelius RJ, Zhang C, Erspamer KJ, Agbor LN, Sigmund CD, Singer JD, et al.: Dual gain and loss of cullin 3 function mediates familial hyperkalemic hypertension. *Am J Physiol Renal Physiol,* 315**:** F1006-F1018, 2018 10.1152/ajprenal.00602.2017
14. Cornelius RJ, Sharma A, Su XT, Guo JJ, McMahon JA, Ellison DH, et al.: A novel distal convoluted tubule-specific Cre-recombinase driven by the NaCl cotransporter gene. *Am J Physiol Renal Physiol,* 319**:** F423-F435, 2020 10.1152/ajprenal.00101.2020
15. McDonough AA, Veiras LC, Minas JN, Ralph DL: Considerations when quantitating protein abundance by immunoblot. *Am J Physiol Cell Physiol,* 308**:** C426-433, 2015 10.1152/ajpcell.00400.2014